Thermoanalytical studies of silver and lead jarosites and their solid solutions

Ray L. Frost · Sara J. Palmer · János Kristóf · Erzsébet Horváth

Abstract Dynamic and controlled rate thermal analysis has been used to characterise synthesised jarosites of formula $[M(Fe)_3(SO_4)_2(OH)_6]$ where M is Pb, Ag or Pb–Ag mixtures. Thermal decomposition occurs in a series of steps. (a) dehydration, (b) well defined dehydroxylation and (c) desulphation. CRTA offers a better resolution and a more detailed interpretation of water formation processes via approaching equilibrium conditions of decomposition through the elimination of the slow transfer of heat to the sample as a controlling parameter on the process of decomposition. Constant-rate decomposition processes of water formation reveal the subtle nature of dehydration and dehydroxylation. CRTA offers a better resolution and a more detailed interpretation of the decomposition processes via approaching equilibrium conditions of decomposition through the elimination of the slow transfer of heat to the sample as a controlling parameter on the process of decomposition. Constant-rate decomposition processes of non-isothermal nature reveal separation of the dehydroxylation steps, since in these cases a higher energy (higher temperature) is needed to drive out gaseous decomposition products through a decreasing space at a constant, pre-set rate.

Keywords Jarosite · Thermal analysis · Controlled rate thermal analysis · Thermogravimetry

Introduction

Argentojarosite ($AgFe_3^{3+}(SO_4)_2(OH)_6$) was first identified in 1923 from the Titanic Standard mine at Dividend, Utah, USA [1]. It has since been identified in at least 14 other US sites. The mineral in some localities is of sufficient abundance as to be a silver bearing ore [2]. Argentojarosite was exploited at Rio Tinto, Spain, from Roman or even pre-Roman times [3]. Argentojarosites had an important influence on the wealth of both Europe and South America [4]. Lead jarosite also known as plumbojarosite ($PbFe_6(SO_4)_4(OH)_{12}$) was identified in relation to jarosite in 1902 [5]. Plumbojarosite is often found in cationic mixed jarosites [6–9]. Such minerals are of importance in medieval and archaeological science [10, 11] and are also found in mine drainage sites both ancient and modern [9, 11, 12]. Such formation of jarosites has been occurring since the Bronze Age [13]. The importance of jarosite formation and its decomposition depends upon its presence in soils, sediments and evaporate deposits [14]. These types of deposits have formed in acid soils where the pH is less than 3.0 pH units [15]. Such acidification results from the oxidation of pyrite which may be from bacterial action or through air-oxidation.

The thermal decomposition of jarosites has been studied for some considerable time [16–20]. However no thermal

R. L. Frost (✉) · S. J. Palmer
Inorganic Materials Research Program, School of Physical and Chemical Sciences, Queensland University of Technology, 2 George Street, GPO Box 2434, Brisbane, QLD 4001, Australia
e-mail: r.frost@qut.edu.au

J. Kristóf
Department of Analytical Chemistry, University of Pannonia, PO Box 158, 8201 Veszprém, Hungary

E. Horváth
Department of Environmental Engineering and Chemical Technology, University of Pannonia, PO Box 158, 8201 Veszprém, Hungary

studies on the pure end member of argentojarosite have been forthcoming, nor has there been studies on argentoplumbojarosites [17]. It has been stated that the thermal decomposition of jarosite begins at 400 °C with the loss of water [21]. The process is apparently kinetically driven. Water loss can occur at low temperatures over extended periods of time [21]. It is probable that in nature low temperature environments would result in the decomposition of jarosite. The products of the decomposition depend upon the jarosite be it K, Na or Pb etc. but normally goethite and hematite are formed together with soluble sulphates [22].

In this work, as part of our studies of secondary mineral formation [23–35] and their stability, we report the comparison of the thermal analysis of designed synthetic lead and silver jarosites using both dynamic and controlled rate thermal analysis techniques.

Experimental

Synthesis of the lead jarosite and argentojarosite

Argentojarosite was synthesised by dissolving 4.8 g $Fe_2(SO_4)_3$ in 120 mL of water. 0.108 g of $AgNO_3$ was added to the solution followed by a further 30 mL of water. The solution was heated in a covered Erhlenmeyer flask for 22 h at 95 °C. The resulting yellow-brown precipitate was collected and dried under vacuum. Powder X-ray diffraction proved the correct structure was obtained.

To synthesise lead jarosite, a 50 mL chloride solution was prepared. This solution contained 0.5 g $PbCl_2$, 12 mL of a saturated LiCl solution and 5 mL of 1.23 M $FeCl_3$ solution. (The high chloride concentration was necessary to prevent the precipitation of lead sulphate). 4.93 g $Fe_2(SO_4)_3$ was dissolved in the minimal volume of water and slowly added drop wise to the chloride solution. The final solution was heated for 21 h at 120 °C in an autoclave. A golden brown precipitate was collected under vacuum and then dried at 100 °C for an hour. 1.25 g of pure lead jarosite was obtained.

The minerals were phase analysed by powder X-ray diffraction and were analysed by chemical composition by EDX methodology.

Thermal analysis

Conventional thermal analysis experiment

Thermal decomposition of the jarosite was carried out in a Derivatograph PC type thermoanalytical equipment (Hungarian Optical Works, Budapest, Hungary) capable of recording the thermogravimetric (TG), derivative thermogravimetric (DTG) and differential thermal analysis (DTA) curves simultaneously. The sample was heated in a ceramic crucible in static air atmosphere at a rate of 5 °C/min.

Controlled rate thermal analysis experiment

Thermal decomposition of the jarosite was carried out in the Derivatograph under static air at a pre-set, constant decomposition rate of 0.1 mg/min. (Below this threshold value the samples were heated under dynamic conditions at a uniform rate of 1.0 °C/min). The samples were heated in an open ceramic crucible at a rate of $1.0\ °C/min^{-1}$ up to 300 °C. With the quasi-isothermal, quasi-isobaric heating program of the instrument the furnace temperature was regulated precisely to provide a uniform rate of decomposition in the main decomposition stage.

Results and discussion

The dynamic TG, DTG and DTA patterns of unground and ground silver, lead and 50:50 and 25–75 lead–silver mixes are shown in Figs. 1, 2, 3, 4 and 5, respectively.
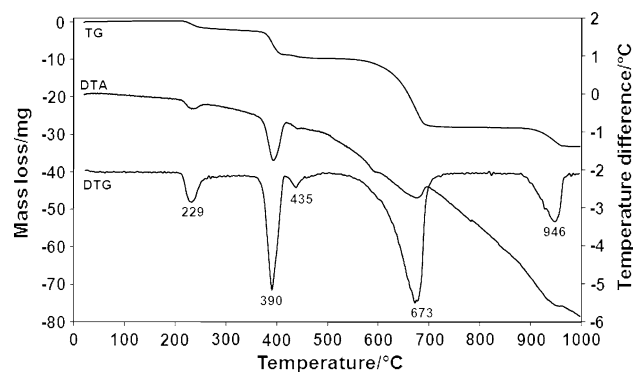

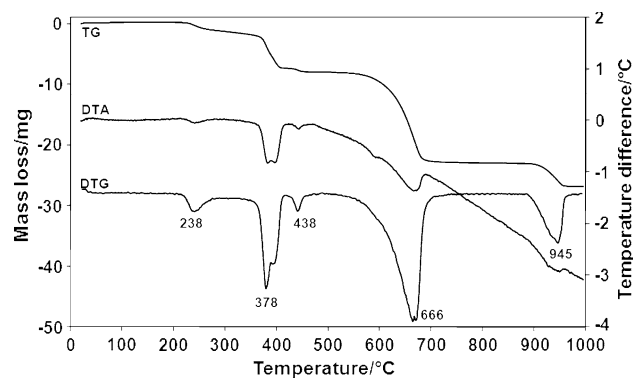Fig. 1 TG, DTG and DTA of unground silver jarosite

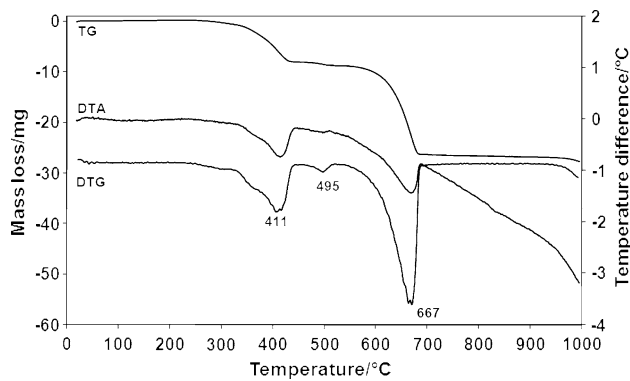Fig. 2 TG, DTG and DTA of ground silver jarosite
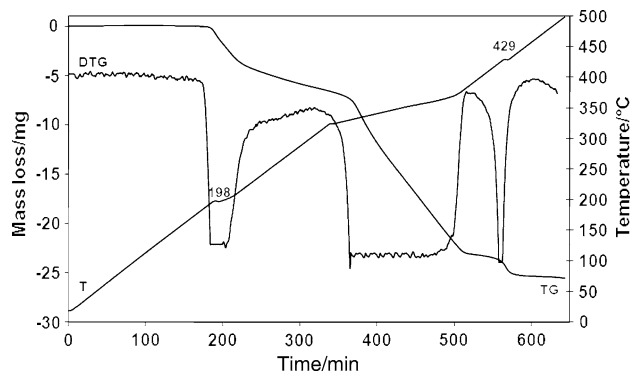
Fig. 3 TG, DTG and DTA of lead jarosite

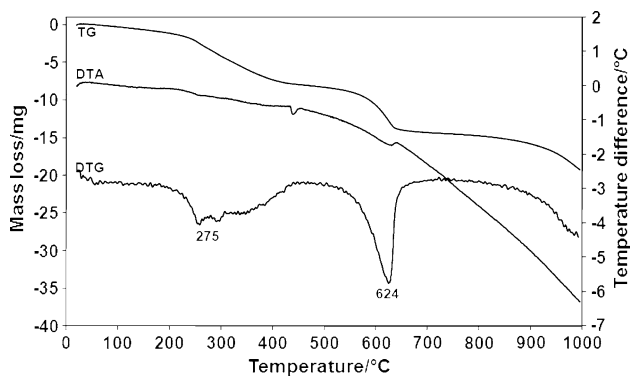Fig. 6 CRTA of unground Ag jarosite

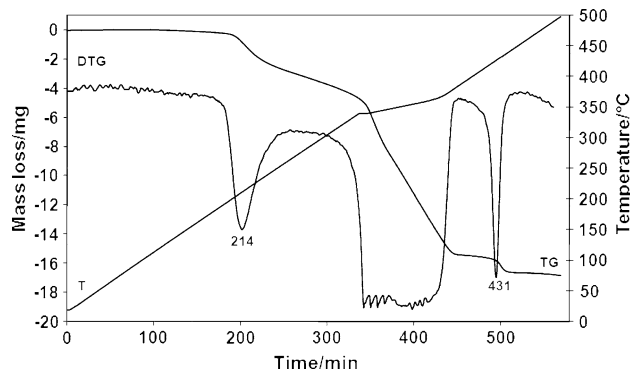Fig. 4 TG, DTG and DTA of lead–silver jarosite (50:50 ratio)
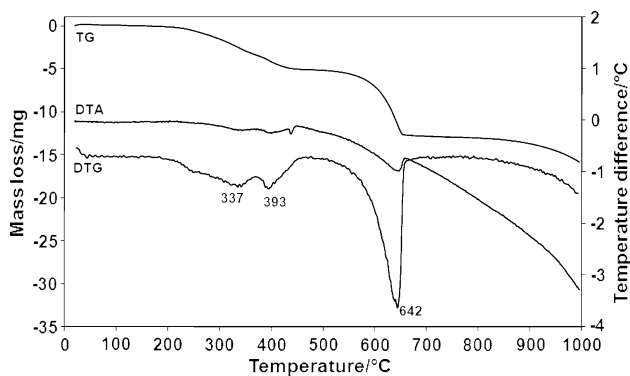

Fig. 7 CRTA of ground Ag jarosite

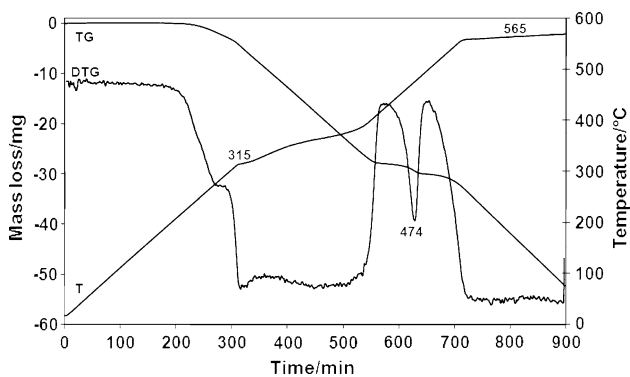Fig. 5 TG, DTG and DTA of lead–silver jarosite (25:75 ratio)

Fig. 8 CRTA of unground Pb jarosite

Dynamic thermal analysis of silver jarosite

The results of the conventional constant rate heating experiment are reported in Table 1. The controlled rate thermal analysis results are reported in Table 2 and the CRTA patterns of unground and ground silver, lead and 50:50 and 25–75 lead–silver mixes are shown in Figs. 6, 7, 8, 9 and 10.

The behavior of the thermal decomposition is different for the silver and lead jarosites and their mixtures. The thermal decomposition of silver jarosite takes place in five mass loss steps as shown in Fig. 1. The mass loss values belonging to the individual decomposition steps are summarized in Table 1. DTG peak maxima are observed at
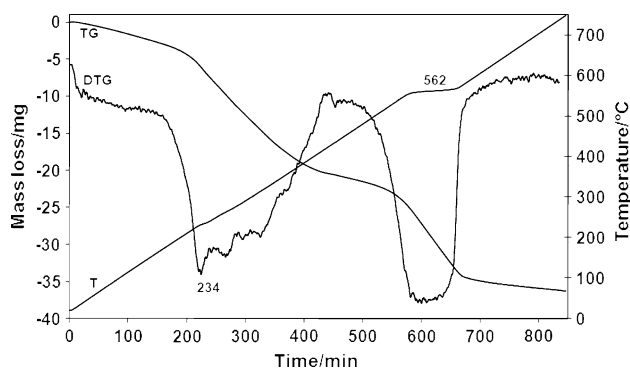
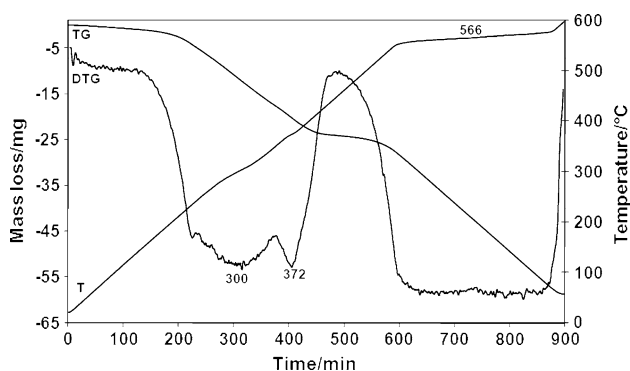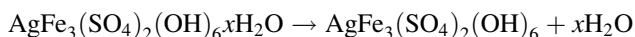**Fig. 9** CRTA of Pb–Ag jarosite (50:50) ratio

Fig. 10 CRTA of Pb–Ag jarosite (25:75) ratio

229, 390, 435, 673 and 946 °C. The DTA patterns shows minima at 230, 395 and 675 °C indicating endothermic steps in the thermal decomposition process.
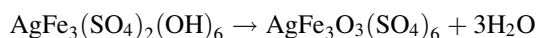
Step 1: dehydration

The loss of crystallization water takes place at 229 °C according to the following equation:

$$AgFe_3(SO_4)_2(OH)_6 x H_2O \rightarrow AgFe_3(SO_4)_2(OH)_6 + x H_2O$$

Based on the TG curve, the exact amount of crystallization water was 1.31 mole.

Step 2: dehydroxylation

Dehydroxylation occurs at 390 and 435 °C resulting in the evolution of 3 moles of water:

$$AgFe_3(SO_4)_2(OH)_6 \rightarrow AgFe_3O_3(SO_4)_6 + 3H_2O$$

(The theoretical mass loss is 13.0%, the observed loss is 11.6%).

Step 3: desulphation

The desulphation reaction occurs in two steps at 673 and 946 °C leading to the formation of $Ag_2SO_4 \cdot Fe_2O_3$ and iron oxide as follows:

$$2AgFe_3O_3(SO_4)_6 \rightarrow Ag_2SO_4 \cdot Fe_2O_3 + 2Fe_2O_3 + 3SO_3$$

(The theoretical mass loss in this reaction is 31.30%, the actual loss is 30.6%).

There is a difference between the unground (Fig. 1) and ground (Fig. 2). In the DTG curve in Fig. 2, peaks are observed at 238, 378 390, 438, 666 and 945 °C. The effect of the grinding on the Ag-jarosite caused an additional peak at 390 °C. The effect of grinding on the DTG peak positions appears to shift the dehydration peak to higher temperatures and the dehydroxylation point to lower temperatures. The first desulphation step is shifted to lower temperatures and the temperature of the second step remains the same. An additional DTA peak at 395 °C is also observed.

Dynamic thermal analysis of lead jarosite

The thermal decomposition behaviour of the lead jarosite (Fig. 3) appears significantly different to that of the silver

Table 1 Decomposition stages under dynamic conditions for jarosites

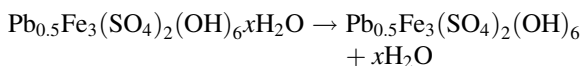| Sample: Ag jarosite unground			Sample: Ag jarosite			Sample: Pb jarosite			Sample: Pb, Ag jarosite			Sample: Pb₂ Ag₈ jarosite		
Temp range/°C	Mass loss (Sample mass: 75.83 mg)		Temp range/°C	Mass loss (Sample mass: 62.78 mg)		Temp range/°C	Mass loss (Sample mass: 75.35 mg)		Temp range/°C	Mass loss (Sample mass: 89.07 mg)		Temp range/°C	Mass loss (Sample mass: 55.13 mg)	
	mg	%		mg	%		mg	%		mg	%		mg	%
204–333	2.5	3.3	200–314	1.6	2.5	242–445	8.2	10.9	30–463	8.1	9.1	68–369	3.5	6.3
333–416	6.5	8.6	314–414	5.9	9.4	445–530	0.7	0.9	463–728	6.4	7.2	369–473	1.7	3.1
416–502	1.0	1.3	414–487	0.7	1.1	530–693	17.6	23.4	728–994	4.8	5.4	473–695	7.7	14.0
502–736	18.3	24.1	487–736	14.9	23.7	693–994	1.4	1.9				695–996	3.1	5.6
875–978	4.9	6.5	883–992	3.8	6.1									

Table 2 Decomposition stages under controlled rate thermal analysis conditions for silver and lead jarosites

Sample: Ag jarosite unground			Sample: Ag jarosite			Sample: Pb jarosite			Sample: Pb, Ag jarosite			Sample: Pb$_2$Ag$_8$ jarosite		
Temperature range/°C	Mass loss (Sample mass: 188.42 mg)		Temperature range/°C	Mass loss (Sample mass: 123.67 mg)		Temperature range/°C	Mass loss (Sample mass: 248.37 mg)		Temperature range/°C	Mass loss (Sample mass: 220.40 mg)		Temperature range/°C	Mass loss (Sample mass: 238.98 mg)	
	mg	%		mg	%		mg	%		mg	%		mg	%
183-306	6.2	3.3	131–291	3.4	2.7	196–331	8.8	3.5	29–425	20.4	9.3	35–349	17.4	7.3
306-389	16.9	9.0	291–388	12.0	9.7	331–421	19.1	7.7	425–701	15.4	7.0	349–443	6.5	2.7
389-467	2.3	1.2	388–455	1.2	1.0	421–498	2.1	0.8				443–593	34.6	14.5
			455–495	0.2	0.2	498–569	21.7	8.7						

jarosite (Fig. 2). The three mass loss steps that appear in the DTG curve at 411, 495 and 667 °C belong to the liberation of water, while desulphation occurs in a single process at 667 °C.
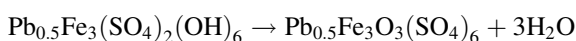
Step 1: dehydration

The loss of crystallization water takes place at temperatures <300 °C according to the following equation:

$$Pb_{0.5}Fe_3(SO_4)_2(OH)_6 xH_2O \rightarrow Pb_{0.5}Fe_3(SO_4)_2(OH)_6 + xH_2O$$

Based on the TG curve, the exact amount of crystallization water was 1.31 mole.

Step 2: dehydroxylation

Dehydroxylation occurs at 411 °C resulting in the evolution of 3 moles of water:

$$Pb_{0.5}Fe_3(SO_4)_2(OH)_6 \rightarrow Pb_{0.5}Fe_3O_3(SO_4)_6 + 3H_2O$$

(The theoretical mass loss is 13.0%, the observed loss is 11.6%).

Step 3: desulphation

The desulphation reaction occurs in a single step at 667 °C leading to the formation of PbSO$_4$·Fe$_2$O$_3$ and alumina as follows:

$$2Pb_{0.5}Fe_3O_3(SO_4)_6 \rightarrow PbSO_4 \cdot Fe_2O_3 + 2Fe_2O_3 + 3SO_3$$

(The theoretical mass loss in this reaction is 33.34%, the actual loss is 36.37%).

Dynamic thermal analysis of silver–lead jarosite

It should be noted that lead and silver jarosites form a continuous series of solid solutions and are identified as a single phases. The thermal analysis patterns of the silver lead jarosites of formula $Ag_{0.5}(Pb_{0.5})_{0.5}Fe_3(SO_4)_2(OH)_6$ xH_2O and $Ag_{075}(Pb_{0.5})_{0.25}Fe_3(SO_4)_2(OH)_6$ xH_2O are given in Figs. 4 and 5. Three mass loss steps are observed over the (a) 30 to 163 °C temperature range assigned to dehydration, (b) the 463 to 728 °C temperature range assigned to dehydroxylation and (c) 728 to 994 °C ascribed to desulphation. For the lead-silver jarosite with equimolar mixtures of silver and lead, the DTG peaks are broad; whereas for the silver-lead jarosite with a 3:1 molar ratio, the DTG peaks are better defined. DTG peaks are observed at 337, 393 and 642 °C. Because silver is the predominant metal in the jarosite, the thermal analysis pattern more closely follows that of the silver jarosite. The effect of the lead is to lower the temperatures of the decomposition steps.

The controlled rate thermal analysis experiment

The thermal decomposition patters of the silver, lead and silver-lead jarosites recorded under CRTA decompositions are shown in Figs. 6, 7, 8, 9, 10. The mass loss data are summarized in Table 2. The dehydration process of silver jarosite (Fig. 6) under the slow heating rate of 1 °C min^{-1} can be resolved to a step between 100 and 200 °C, at 198 °C. During the dynamic experiment only two dehydration steps could be identified in the DTG curve. The controlling rate of 0.1 mg min^{-1} was not reached until 375 °C. Dehydroxylation took place in a homogeneous process represented by an isothermal, constant rate of water evolution at 375 °C. The CRTA of the ground Ag-jarosite (Fig. 7) provided a different pattern. A non-isothermal step assigned to dehydration is observed at 214 °C. In this case the dehydroxylation took place at 400 °C in an isothermal process.

Dehydration of lead jarosite (Fig. 8) under CRTA conditions took place in two steps (similarly to the dynamic experiment) up to 200 min and between 200 and 400 min.

The controlling level of 0.1 mg min^{-1} was reached in both steps resulting in a quasi-isothermal pattern of water evolution at 80 and 150 °C. Above 400 min, dehydroxylation took place in four steps at 200, 249, 325 and 452 °C under the slow heating (the rate of decomposition did not reached the controlling level of 0.1 mg min^{-1}). This experiment revealed the subtle nature of dehydroxylation which was not observed in the dynamic experiment.

The thermal decomposition of the silver-lead mixed jarosites (Figs. 9 and 10) under CRTA conditions results in dehydration occurring in a series of non-isothermal steps up to 300 °C. A quasi-isothermal steps is observed at 562 °C, attributed to desulphation. For the $Ag_{075}(Pb_{0.5})_{0.25}Fe_3(SO_4)_2(OH)_6$ xH_2O jarosite two dehydroxylation steps are observed similar to the two dehydroxylation steps observed in the dynamic experiment. A pseudo-isothermal desulphation step at 566 °C is observed (Fig. 10).

Conclusions

Synthetic jarosites show characteristic thermogravimetric patterns with thermal decomposition steps: (a) dehydration, (b) well defined dehydroxylation and (c) desulphation. While the patterns of dehydration and dehydroxylation (as well as the amounts of crystallisation water) differ significantly depending on the nature of the cation, desulphation is a rather homogeneous process (the DTG peak temperatures fall in the range between 760 and 800 °C for all the five samples).

CRTA offers a better resolution and a more detailed interpretation of the decomposition processes via approaching equilibrium conditions of decomposition through the elimination of the slow transfer of heat to the sample as a controlling parameter on the process of decomposition. With this technique differences in the dehydration and decomposition patterns can be revealed suspecting a more complex pattern of decomposition as revealed under dynamic hating.

It is very important to be able to thermally characterise minerals such as jarosites which may be found on planets such as Mars. The existence of jarosites on Mars would confirm the presence of water at some time in the past as such minerals are only formed from solution. The thermal stability of jarosites is most important as there is a need to find the temperature range over which the minerals are stable, since wide temperature ranges are likely on planets.

References

1. Schaller WT. Argentojarosite, a new silver mineral. J Wash Acad Sci. 1923;13:233.
2. Schempp CA. Argento-jarosite: a new silver mineral. Am J Sci. 1923;6:73–5.
3. Dutrizac JE, Jambor JL, O'Reilly JB. Man's first use of jarosite: the pre-Roman mining-metallurgical operations at Rio Tinto, Spain. Can Inst Min Metall Bull. 1983;76:78–82.
4. Dutrizac JE, Jambor JL. Jarosites and their application in hydrometallurgy. Rev Miner Geochem. 2000;40:405–52.
5. Hilebranad WF, Wright FE, New A. Occurrence of plumbojarosite. Am J Sci. 1910;30:191–2.
6. Leach FI. Plumbojarosite-a little-known mineral. Min J. 1937;20:40.
7. Mumme WG, Scott TR. The relationship between basic ferric sulfate and plumbojarosite. Am Min. 1966;51:443–53.
8. Dutrizac JE, Dinardo O, Kaiman S. Factors affecting lead jarosite formation. Hydrometallurgy. 1980;5:305–24.
9. Taberdar T, Gulensoy H, Aydin AO. Plumbojarosite mineral found in Bolkardag mines [Turkey] by TGA, DTA, and X-ray diffraction, Marmara Universitesi Fen Bilimleri Dergisi 2, 1985. p. 76–93.
10. Amoros JL, Lunar R, Tavira P. Jarosite: a silver-bearing mineral of the gossan of Rio Tinto (Huelva) and La Union (Cartagena, Spain). Mineralium Deposita. 1981;16:205–13.
11. Rewitzer C, Hochleitner R. Minerals of the old slags from Lavrion, Greece (Part 2), Rivista Mineralogica Italiana, 1989. p. 83–100.
12. Harris DL, Lottermoser BG, Duchesne J. Ephemeral acid mine drainage at the Montalbion silver mine, north Queensland. Aust J Earth Sci. 2003;50:797–809.
13. Hudson-Edwards KA, Schell C, Macklin MG. Mineralogy and geochemistry of alluvium contaminated by metal mining in the Rio Tinto area, southwest Spain. App Geochem. 1999;14:1015–30.
14. Buckby T, Black S, Coleman ML, Hodson ME. Fe sulfate-rich evaporative mineral precipitates from the Rio Tinto, southwest Spain. Min Mag. 2003;67:263–78.
15. Williams PA. Oxide zone geochemistry. Chichester, West Sussex, England: Ellis Horwood Ltd; 1990.
16. Nagai S, Yamanouchi N. Potassium ore jarosite. I. Properties of jarosite and leaching test of potassium portion, Nippon Kagaku Kaishi (1921-47) 52 (1949) 83–86.
17. Kulp JL, Adler HH. Thermal study of jarosite. Am J Sci. 1950;248:475–87.
18. Cocco G. Differential thermal analysis of some sulfate minerals. Periodico di Mineralogia. 1952;21:103–38.
19. Tsvetkov AI, Val'yashikhina EP. Thermal characteristics of minerals of the alunite group. Doklady Akademii Nauk SSSR. 1953;89:1079–82.
20. Tsvetkov AI, Val'yashikhina EP. Phase conversions of hydrated iron sulfates (fibroferrite, $Fe(SO_4)(OH).4.5H_2O$, and melanterite, $FeSO_4·7H_2O$) by heating. Doklady Akademii Nauk SSSR. 1953;93:343–6.
21. Dutrizac JE, Jambor JL. Reviews in mineralogy and geochemistry Volume 40. In: Alpers CN, Jambor JL, Nordstrom DK, editors. Chapter 8 Jarosites and their application in hydrometallurgy; 2000. p. 405–452.
22. Thomas PS, Hirschausen D, White RE, Guerbois JP, Ray AS. Characterization of the oxidation products of pyrite by thermogravimetric and evolved gas analysis. J Therm Anal Calorim. 2003;72:769–76.
23. Frost RL, Hales MC, Martens WN. Thermogravimetric analysis of selected group (II) carbonate minerals—implication for the

geosequestration of greenhouse gases. J Therm Anal Calorim. 2009;95:999–1005.

24. Palmer SJ, Spratt HJ, Frost RL. Thermal decomposition of hydrotalcites with variable cationic ratios. J Therm Anal Calorim. 2009;95:123–9.

25. Carmody O, Frost R, Xi Y, Kokot S. Selected adsorbent materials for oil-spill cleanup. A thermoanalytical study. J Therm Anal Calorim. 2008;91:809–16.

26. Frost RL, Locke A, Martens WN. Thermogravimetric analysis of wheatleyite $Na_2Cu^{2+}(C_2O_4)_2 \cdot 2H_2O$. J Therm Anal Calorim. 2008;93:993–7.

27. Frost RL, Locke AJ, Hales MC, Martens WN. Thermal stability of synthetic aurichalcite. Implications for making mixed metal oxides for use as catalysts. J Therm Anal Calorim. 2008;94:203–8.

28. Frost RL, Locke AJ, Martens W. Thermal analysis of beaverite in comparison with plumbojarosite. J Therm Anal Calorim. 2008;92:887–92.

29. Frost RL, Wain D. A thermogravimetric and infrared emission spectroscopic study of alunite. J Therm Anal Calorim. 2008;91:267–74.

30. Hales MC, Frost RL. Thermal analysis of smithsonite and hydrozincite. J Therm Anal Calorim. 2008;91:855–60.

31. Palmer SJ, Frost RL, Nguyen T. Thermal decomposition of hydrotalcite with molybdate and vanadate anions in the interlayer. J Therm Anal Calorim. 2008;92:879–86.

32. Vagvoelgyi V, Daniel LM, Pinto C, Kristof J, Frost RL, Horvath E. Dynamic and controlled rate thermal analysis of attapulgite. J Therm Anal Calorim. 2008;92:589–94.

33. Vagvolgyi V, Frost RL, Hales M, Locke A, Kristof J, Horvath E. Controlled rate thermal analysis of hydromagnesite. J Therm Anal Calorim. 2008;92:893–7.

34. Vagvolgyi V, Hales M, Martens W, Kristof J, Horvath E, Frost RL. Dynamic and controlled rate thermal analysis of hydrozincite and smithsonite. J Therm Anal Calorim. 2008;92:911–6.

35. Zhao Y, Frost RL, Vagvolgyi V, Waclawik ER, Kristof J, Horvath E. XRD, TEM and thermal analysis of yttrium doped boehmite nanofibres and nanosheets. J Therm Anal Calorim. 2008;94:219–26.